Characterization of a support-free carbon nanotube-microporous membrane for water and wastewater filtration

Chidambaram Thamaraiselvan[a], *Sofia Lerman*[a], *Kamira Weinfeld-Cohen*[b], *Carlos G. Dosoretz*[a*]

[a]Faculty of Civil and Environmental Engineering and Grand Water Research Institute, Technion Israel institute of technology, Haifa 3200003, Israel

[b]Surface Science Laboratory at the Solid State Institute, Technion Israel Institute of Technology, Haifa, 3200003, Israel

[*]Corresponding author: E-mail address: carlosd@technion.ac.il.

Abstract

Nonwoven carbon nanotube (CNT) laminates were characterized as support-free membranes for water filtration in terms of structural morphology, water permeability, selectivity and chemical resistance. Nominal pore rating (12-23 nm) estimated by rejection of globular proteins and fluorescence beads fall within the selectivity range of tight ultrafiltration (UF) membranes applied for wastewater treatment. The membranes displayed high permeability (120-400 LMH/bar). High selectivity regardless of high permeability seems to be due to tortuosity and pore structure of the membranes (25-50 μm thickness). The chemical stability of the membranes was tested towards common chemicals used for membrane cleaning (HCl, NaOH, NaClO) but at much severe conditions (24 h exposure at 4-10 fold higher concentrations). High resolution-X-ray photoelectron spectroscopy (XPS) was applied to evaluate chemical resistance. The relative C/O-carbon to oxygen ratio and typical deconvolution curves of C1s lines of the membranes after 24 h exposure depicted no significant changes compared to the reference samples, confirming resistance to chemical oxidation. This combination of features, added to simplicity of fabrication and post-synthesis modification and support-free configuration that enhances chemical stability, offer a worthwhile opportunity of application of these dense-array outer-walled CNT membranes in the UF range, especially at harsh conditions such as wastewater treatment.

Keywords: Support-free membrane; Carbon nanotube laminates; High flux-membranes; Chemical resistance; Wastewater treatment

1. Introduction

Carbon nanotubes (CNT)-based membranes either standalone or embedded into a polymeric composite matrix, is an emerging area of research and development. Intrinsic properties of CNT comprise high physical properties and resistance to chemicals, combined with electrical conductivity and ductility [1-3]. The importance as well as impact of application of CNT membranes in water and especially wastewater treatment is tremendous [4]. Recent reports show that CNT membranes have good antibacterial activity as well, which is dependent on the CNT size structure and additional attached groups [5-7]. A few works review the molecular modeling and experimental aspects of CNT membrane fabrication and functionalization and also proper manufacturing methods of CNT composite membranes for the desalination of sea and brackish water [8, 9]. Performances of CNT composite membranes were evaluated with different polymers such as polyvinylidine fluoride (PVDF) [10] and novel type of polyelectrolyte complex [11]. Also multi-walled carbon nanotubes (MWCNT) incorporated in ceramic composite membranes strongly inhibited the propagation of bacteria on the filters with an antibacterial rate of almost 98% [12]. In addition to antibacterial and antifouling properties, the overall performance of CNT composite membranes was also increased when mixing with other nanoparticles such as graphene oxide (GO) [13] and silver nanoparticles [14, 15].

In general terms four different kind of CNT membranes have been reported for water separation (or purification) [4]: (i) Template synthesized CNT membranes, consisting on deposition of carbonaceous materials inside preexisting ordered porous templates, e.g., anodized alumina; (ii) Dense-array outer-wall CNT membranes, based on the interstice between nanotubes in a vertical or random array distribution of CNTs; (iii) Open-ended CNT membranes based on encapsulation of as-grown vertically aligned CNTs by a space-filling inert polymer or ceramic matrix; (iv)

Mixed-matrix membranes composed of nanotubes as fillers in a polymer matrix. Water molecules move through CNT pores orders of magnitude faster than through other pores of comparable size. Many features seem to influence water transport along and/or across CNTs, such as molecularly smooth hydrophobic graphitic walls, nanoscale inner diameters, diameter to length ratio of CNTs, etc. Water molecules were occasionally observed to move along the nanotube axis via bursts of hydrogen-bonded clusters of molecules [16, 17]. In CNTs with smaller diameters, however, water molecules have been shown to assemble into diameter-dependent one-dimensional structures [4]. Nevertheless, the mechanism of separation is complex and not yet completely defined. Srivastava et al. [17] attributed the filtration process driven by gravity of a membrane made of dense-array outer-wall CNTs to the geometry of the nanotubes, their nanoporosity and the selective adsorption of the nanotube surfaces. Since the inter-tubular spaces dominated the porosity in the membrane, they concluded that most of the filtering occurs in the interstitial spaces, although some transport through the inner hollow channels of the tubes cannot be ignored.

Among various types of CNT membranes for water purification, the feasibility of vertically aligned (VA) CNT membranes was recently reported [18]. Two types of VA CNT membranes has been used, one is open-ended CNT which implies opened CNT tips [19, 20] and another is outer wall membrane [20-22], in which the interstices between nanotubes in a vertically array of CNT were considered as pores. The pure water flux of VA CNT membrane significantly increased approximately three times higher than the UF membrane. Additionally, the VA CNT membrane displayed good biofouling resistance with approximately 15% less permeate flux reduction and 2 log less bacterial attachment than the UF membrane [18]. Very high water permeability was reported up to 30,000 LMH/bar using VA CNT wall hollow fiber membranes

[20]. CNT hollow fiber membranes with a water flux of 12,000±500 LMH (was fabricated by wet spinning technology [23]. However, it is quite obvious that still significant challenges have to be addressed to align the CNTs, to reinforce them in a suitable host matrix without disturbing the alignment and inhibiting the agglomeration (adoption of suitable nanocomposite fabrication route), to open the tips preferentially and to scale up favorably [4]. Moreover, composite CNT membranes are deprived of the strong chemical and thermal resistance of CNTs as well as a considerable loss of electrical conductivity. Direct spinning of CNT fibers from a chemical vapor deposition (CVD) synthesis zone of a furnace using a liquid source of carbon and an iron nano-catalyst was reported [24]. This direct spinning from a CVD reaction zone is extendable to the production of nonwowen laminates. CNT membranes are not yet commercialized due to lack of high throughput fabrication technologies. To best of our knowledge, the first commercial product using CNT rolled in a depth filter structure was launched by Seldon [25].

The objective of this study is to evaluate the performance of CNT laminates of significantly long tubes, fabricated using the direct spinning method from the CVD processes, as support-free microporous membranes. Very simple post-synthesis modification of the laminates allowed control of permeability and selectivity. A detailed characterization of the CNT membranes in terms of permeability, selectivity, resistance to the chemicals, pore rating, zeta potential, contact angle and tortuosity is presented.

2. Materials and methods

2.1 CNT laminates and conditioning

The CNT laminates evaluated were kindly supplied by Tortech Nano Fibers (TNF) and made using an established protocol [24]. Carbon nanotubes were fabricated using direct spinning from the chemical vapor deposition synthesis zone of a furnace in which a continuous gas phase

catalytic reaction between a floating Fe-catalyst and a liquid source of carbon takes place. By mechanically drawing the CNT from the gaseous reaction zone with a rotating spindle enables the formation of ultra-long CNTs (~2 mm), achieving in turn the formation of a continuous and robust non-woven mat. The alignment of the nanotubes and the thickness of the coatings were controlled by the rotation speed and coating time.

Different batches of fibers were fabricated by changing the flow rate of iron catalyst. A list of the laminates tested is presented in Table 1. In batch C171, the total carbon flow was 1.5 times more than batch C80, and in batch C162 the catalyst total flow was 1.33 times lower than batch C80. Most part of the study was carried out with C80 laminates. Three type of laminates were tested: (i) unmodified; (ii) stretched (str); (iii) acetone densified (actD). Laminates modifications by either stretching or acetone condensation were performed in order to increase laminate density and surface homogeneity. Unmodified and stretched (10%) laminates were supplied by Tortech. Acetone densification was performed by soaking pristine laminates in acetone for 5 min which were immediately dried at 70ºC in an oven for 10 min. Prior to their use, all membranes were soaked in double distilled water (DDW) for about 12 h and then carefully washed with a 70% ethanol solution to reduce any endogenous contamination (aseptic conditions). Ultimate tensile strength (UTS) and strain to failure ratio of the CNT unmodified laminates were in the range of 70-100 MPa and approx. 15%, respectively. Stretched laminates (~10%) have an increase of ~50% in UTS and a ~50% decrease in the strain ratio (Tortech Nano Fibers).

2.2 Permeability tests

Permeability tests were performed with DDW using 50 mL Amicon® stirred filtration cells (Millipore) with a variable pressure between 0-1 bar, at a 0.25 bar interval. Permeate flux was

calculated according to Eq. (1). Water temperature was measured before and after every filtration and the permeation results were normalized to 20ºC according to Eq. (2):

$$J^T = \frac{Q}{A} \qquad (1)$$

$$J^{20} = J^T \times \frac{\mu^T}{\mu^{20}} \qquad (2)$$

where: Q-volumetric flow rate [m^3/h]; A- filtration area [m^2]; J^T and J^{20}- permeate flux at temperature T and 20ºC, respectively [L/m^2.h]; μ^T and μ^{20}- dynamic viscosity at temperate T and 20ºC, respectively [cP].

Normalized permeability at 20ºC (L_p^{20}) was calculated from the slope of the plot of J^{20} vs. ΔP according to Eq. (3):

$$J^{20} = J_o^{20} + \Delta P \times L_p^{20} \qquad (3)$$

where L_p^{20} is expressed in L/m^2.h.bar; J_o^{20} - intrinsic flux at ΔP=0 [L/m^2.h]; ΔP- transmembrane pressure [bar].

Permeability tests were repeated at least three times. Each permeability point was tested at least in triplicates.

2.3 Selectivity tests

Selectivity tests aimed at defining the pore rating of the membranes were performed with globular protein markers and fluorescent polystyrene beads. The tests were performed using 50 mL Amicon (Millipore) stirred cells described above, applying a pressure of 1 bar following ASTM E1343-90 [26] with some modifications.

2.3.1. Rejection of protein markers

Selectivity tests were mainly performed by measuring the rejection of a protein mix standard of known molecular size (AL0-3042, Phenomenex) supplemented with bovine serum albumin (BSA) and blue dextran (BD) (Sigma-Aldrich) and assayed by gel filtration chromatography (GFC). BD was used as void volume marker for the GFC. Markers solution was prepared in filtered (0.22 µm filter, Millipore) DDW. The components, concentration and molecular size of each marker in the whole mixture are shown in Table S1 (supplementary information).

Prior to start of the experiments all tested membranes were profusely rinsed with double distilled water (DDW) and soaked in a 1 g/L BSA solution in order to prevent adsorption of the proteins markers onto the membranes [27]. The samples collected from the Amicon cells were filtered once again using a 0.2 µm Teflon syringe filter (17 mm, National Scientific) and analyzed by GFC on UV-HPLC.

The hydrodynamic diameter (d_H) of the proteins, all globular, was calculated as spherical model [28] as presented in Eq. (4):

$$d_H = 0.132 \times MW^{0.33} \qquad (4)$$

and for blue dextran was calculated based on the model of a linear molecule [28] as presented in Eq. (5):

$$d_H = 0.11 \times MW^{0.46} \qquad (5)$$

where MW is the molecular weight in Da and d_H is given in nm.

2.3.2. Rejection of fluorescent beads

Membrane rejection in the size range of 40-900 nm was also tested using polystyrene fluorescent beads (Spherotech) with different fluorophores, each color representing a different size. The beads specifications are presented in Table S2 (supplementary information). Beads concentration in all stock suspensions was 1% w/v. The experimental setup consisted of two solutions, the first

one contained three colors, blue (diluted 1:100), pink and yellow (both diluted 1:200). The second solution contained the nile red color- diluted 1:200 also. The nile red color was masked by the other colors so it had to be used separately. The final volume of each solution was 10 ml. Each membrane was tested with this solution using the Amicon stirred cells at a 1 bar pressure as described above. A sample of 150 µL was taken from the permeate of each membrane and placed in a FluoroNanc 96 wells white plate (Nunclon, Thermo Scientific). The fluorescence bands were measured by an Infinite M200 Pro multimode reader (Tecan). DDW was used as blank.

2.3.3. Pore rating determination

The pore rating for a spherical molecule was calculated from the Ferry-Renkin equation [29], Eq. (6):

$$R = \left[1 - 2\left(1 - \frac{d_H}{d_m}\right)^2 + \left(1 - \frac{d_H}{d_m}\right)^4\right]\left[2.104\left(\frac{d_H}{d_m}\right) - 2.09\left(\frac{d_H}{d_m}\right)^3 + 0.95\left(\frac{d_H}{d_m}\right)^5\right], d_H \le d_m \qquad (6)$$

where R [dimensionless] is the rejection of a spherical particle (either globular proteins or polystyrene beads) and d_m [nm] is the membrane pore diameter (or absolute pore rating). The term on the right-hand side of Eq. (6) describes the rejection of spherical particles due to steric screening at membrane pore entrance; the second term is associated with hindered convection of particles inside membrane pores. $R \equiv 1$ for any $d_H > d_m$. Nominal pore rating and molecular weight cut off (MWCO) were drawn at 90% rejection from the semi-logarithmic plot of rejection vs. hydrodynamic rate or molecular weight, respectively.

2.4. Chemical resistance tests

In order to evaluate the chemical resistance of the CNT membranes, experiments were carried out applying solutions of common chemicals used for chemical cleaning and cleaning in place

(CIP) during typical membranes operation, but at harsher conditions (higher concentrations and/or longer exposure time): 2 N HCl, 2 N NaOH and a 0.5-2 g/L NaOCl. Exposure lasted for 24 hours and samples were taken at time 0, 1 and 24 hours. The effect of the chemical treatment on the CNT membranes was tracked by permeability measurement with DDW and X-ray photoelectron spectroscopy (XPS) characterization (relative C and O content) to determine the possible changes in chemical composition. For the C-80 membranes, selectivity was also tested following the chemical resistance tests in order to estimate the potential effect on chemical cleaning on the overall membrane performance (permeability and selectivity).

The exposure to the cleaning chemicals was performed as follows. Several coupons (replicates) of each membrane were soaked in the indicated solution for the indicated time in Petri dishes. Then coupons were sampled, thoroughly washed in DDW and tested for permeability, selectivity and XPS. Tests were repeated at least three times. Permeability was tested with DDW in the stirred cells mentioned above water under pressure of 1 bar (see section 2.2). Selectivity was performed using the protein markers as described in section 2.3.1.

2.5. Flow-through experiments

A flow-through cells system with internal recirculation operating in continuous mode was used to test permeability and antibacterial activity of the C-80 CNT membranes. Flow conditions and experimental set-up were as described in our previous works [3, 30]. Antibacterial tests were performed comparatively to polysulfone (Psf) 200 KDa UF membranes (ymersp3001, GE Osmonics) under conditions encouraging biofouling. Permeability were monitored until Psf membrane reached baseline. At the end of the experiments, the membranes were removed and visualized by HRSEM microscopy.

2.6. Analytical techniques

Established analytical techniques were applied for characterization of the membrane surface and properties, comprising HR-SEM microscopy and tortuosity estimation [31, 32], atomic force microscopy (AFM) [33], contact angle analysis, zeta potential analysis, gel filtration chromatography and X-ray photoelectron spectroscopy. Detailed information is supplied in the supplementary information (Section S1).

3. Results and discussion

3.1. Water permeability and selectivity

The normalized water permeability values of the different CNT membranes tested in this research are shown in Fig. 1. A summary of the average normalized permeability is presented in Table 1. As shown in the data presented all unmodified membranes displayed very high permeability which was somewhat reduced upon modification by either stretching or acetone densification. Although the unmodified membranes displayed higher permeability, they also showed a higher variation denoting the lack of uniformity of the membranes, which was reduced by post-synthesis modification. Overall, a water permeability higher than most commercially available polymeric UF membranes applicable for water/wastewater treatment was observed in all the CNT membranes. This high permeability is most probably due to the inherent morphology of the CNT membranes and the pore geometry determined by the dense-array of the smooth graphitic outer-wall of the tubes, granting a high nanoporosity, in line with previous observations [17]. Although some water transport through the inner hollow channels of the tubes via hydrogen-bonded clusters cannot be ignored, most of the filtration seems to occur through the inter-tubular spaces dominating the porosity in the membrane [4].

As seen in the data presented, the linear fit does not crossed the axis intersection indicating that water may permeate through these membranes even without applied pressure (i.e., intrinsic flux).

Intrinsic flux or seepage phenomena in dense-array outer-wall CNT membranes is common [17]. In order to hinder this behavior, two modifications were performed to the membranes i.e., 10% mechanical stretching and acetone densification (Figs. 1B and 1C, respectively). The modified CNT membranes displayed reduced intrinsic flux by 1-2 folds. In addition, these modifications enhanced selectivity and decreased tortuosity (see below). Even though modifications decreased permeability compared to the unmodified membranes, it still remained high compared with most commercial polymeric UF membranes in line with previous reports [10, 18, 23]. Permeability of C-80 unmodified membranes was also tested in cross-flow regime in bench scale flow-through cells. The average steady state permeability was 416±62 LMH/bar for six independent replicates, in line with the values in dead-end mode.

The selectivity of all membranes studied, characterized by nominal pore rating using a mixture of fluorescent polystyrene beads (40-860 nm) and globular protein markers (17-2,000 kDa), are presented in Tables 1 and 2. It can be seen that all the membranes displayed a nominal pore rating in the range of highly selective ultrafiltration membranes applied for water/wastewater treatment (12-23 nm). As an example, the MWCO plot for the unmodified C-80 membrane is presented in Fig. 2. As shown in the graph, C-80 membrane displays complete rejection of proteins larger than 150 kDa (IGg) with a MWCO at 65 kDa corresponding to a nominal pore rating of 23 nm calculated according to Ferry-Renkin equation [29]. This pore size fits well in the tightest UF membrane range applied for water/wastewater treatment. When considering the permeability of the membranes ranging from 120-400 LMH/bar (see Fig. 1), the CNT membranes present a worthwhile combination of high permeability and high selectivity, compared to most commercial UF membranes. The MWCO plots for the modified C-80 membranes are presented in Fig. S1. This high selectivity regardless of the high permeability can

247 be most probably regarded to adsorption and intrinsic tortuosity across the whole thickness of the
248 non-woven membranes (by average 25-50 μm), acting as self-supporting membranes, in line
249 with previous reports [4].
250 When compared to CNT-composites, the CNT membranes showed two to four folds higher
251 permeability. For instance, about 53 LMH/bar pure water flux were reported in PES/NH_2-
252 MWCNT nanocomposite UF membrane [34]. Many works reported flux values of composite
253 membranes in the range of ultrafiltration, for example, flux of 205 LMH/bar for
254 Ag/MWCNT/PAN hollow fiber composite membrane with pore size in the range of 2-5 nm [15]
255 and 109 LMH/bar for a composite hollow fiber membrane with 7.1 to 8.4 nm of pore size [35].
256 In contrast, quite higher flux of about 5700 LMH was reported in the composite hollow
257 membrane in the range of tight ultrafiltration (capable of complete removal of 10 nm particles)
258 [36]. Nevertheless, the simplicity of fabrication and easy of post-synthesis modification of the
259 dense-array outer-wall CNT membranes presented here, added to support-free configuration that
260 enhances chemical and temperature stability owning high electrical conductivity [3], make them
261 especially suited for harsh application conditions in wastewater treatment and purification
262 (effluents filtration, membrane bioreactor-MBR).
263 ***3.2. Morphology of CNT membranes***
264 Detailed structural characterization of the C-80 membranes is presented in Figs. S1 and S2
265 (supplementary information) and Table 2. HR-SEM micrographs of both top layer-surface (Fig.
266 S2 A-C) and cross section (Fig. S2 D-F) of well-aligned unmodified C80 membranes at different
267 magnifications ranging from 5 to 300 kX are shown. As seen from these micrographs, dense
268 CNT fibers entangled multi-directionally, consisting of curved tubes could be noticed.
269 Comparative HR-SEM micrographs of unmodified, stretched and acetone densified C-80

membranes at a magnification of 30kX are presented in Fig. S3 A-C. Hence, a thin section of the top layer was carefully peeled off from the membranes and imaged (Fig. S3 D-F), depicting the shape of the CNT fibers. The curvature of the fibers is indicative of the tortuosity of the pores. The tortuosity factor (l_o/l_e), defined as the ratio of the length of the curved line between two points-l_o (red lines in Fig. S3 D-F) to the linear distance between the two points-l_e (white lines in Fig. S3 D-F), was evaluated according to Zhou et al. [31]. The tortuosity of the each layer was measured at least in six different places summing 20 independent replicates. The calculated tortuosity factor of unmodified membranes exhibited larger values (2.8±1.4) than the modified membranes, 2.4±1.5 for stretched and 1.8±0.5 for acetone densified (Table 2). As seen for these results, the tortuosity can be altered and manipulated by either chemical or mechanical densification, in line with previous reports [20, 32]. Tortuosity seems correlated to permeability, probably related to the densification of the membranes, which decreased tortuosity and in turn permeability. Indeed, unmodified C-80 which displayed the highest tortuosity resulted in the highest permeability (352±60 LMH) (see Table 1).

The AFM topography of CNT membranes is presented in Fig. S4. It can be seen that all these CNT membranes exhibited a uniform structure (Fig. S4-top). The measured electrostatic force curves of the three CNT membranes are shown in Fig. S4-bottom. The calculated repulsive forces of C-80, C-80 str and C-80 actD at a distance of 2 μm were greater than 21 nN, 54 nN and 35 nN respectively and converged less than the 9 nN at 600 μm. Indeed, repulsive forces are very short-range forces and display an exponential or inverse power decaying profile with distance. The average roughness and root mean square (RMS) are shown in Table 2. In agreement with the repulsive forces, both roughness (34.2±3.0) and RMS (43.5±3.5) of C-80 str displayed the largest values. In general, the roughness of the CNT membranes was slightly

higher than reported values for VA CNT membranes [18], as was the tortuosity factor. Remarkably, AFM data inversely correlated contact angle, selectivity (see Table 2) and thickness (see Table 1) of the membranes. The lowest contact angle was observed for C-80% str (78.3±7.12 ˚θ) corresponding to a highest roughness and better selectivity (MWCO at 18 kDa) and smallest thickness (25 μm), compared to unmodified C-80 (102.2±6.7 ˚θ) and C-80 actD (118.1±9.1˚θ). The more hydrophilic C-80 membranes, unmodified and actD, displayed a somewhat lower selectivity (MWCO at 65 and 26 kDa, respectively) in correspondence to a smaller roughness. Noticeable, the more hydrophilic unmodified C-80 displayed the highest permeability. The measured zeta potential of the unmodified C-80 membrane was -43.5±4.9 mV at pH 7, this negative charge might be influence strongly on the rejection of negatively charged species. The intrinsic hydrophobic nature of CNT membranes is attributed to the low surface energy of CNT [34], which could benefit the mitigation of membrane fouling in the cross-flow filtration mode. The adsorption of foulants on a low-energy surface is normally weak and can be easily rinsed-off by the shearing forces of the cross-flowing feed solution.

3.3. Chemical resistance of CNT membranes

Chemical resistance tests were performed in order to evaluate the behavior of the membranes to chemical treatments applied for routine cleaning and CIP during membrane operation, but under extreme conditions (higher concentrations and/or longer exposure time). The relative permeability values of all membranes after the treatment with 2 N NaOH, 2 N HCl and 500-2000 mg/L of NaOCl are presented in Table 3. The results indicate that permeability of all the membranes was only slightly influenced by long terms exposure to the concentrated chemicals (up to 5%). Some membranes exhibited a decrease in the permeability as a result of a specific treatment, for example C-171 str displayed a decrease in the permeability after the treatment with

316 2 g/L NaClO. In most of the cases though, an increase in the permeability was observed,
317 especially after 24 h of exposure to the chemicals, as in the case of C-162 actD after the
318 treatment with 2 N HCl. Interestingly, the treatment of 2 N NaOH caused the steadiest increase
319 of permeability to all the membranes.
320 A more comprehensive evaluation of chemical resistance was performed for the C-80
321 membranes. The relative permeability data is presented in the three bottom rows of Table 3, the
322 effect on the nominal pore rating in Fig. 3 and XPS data in Fig. 4 and Tables 4 and 5. As seem
323 from the results presented, no significant changes in the permeability were found among the
324 treatments, although some increase in the permeability was observed especially after 24 h of
325 exposure to HCl and NaOH (see Table 3). Regarding selectivity, in most of the cases the
326 treatments improved the nominal pore rating that resulted in better rejection of the markers (see
327 Fig. 3). This behavior might be explained by increased van der Waals interaction between CNT
328 fibers upon treatment (similar to the acetone densification that was made as pretreatment)
329 resulting in a higher rejection, thus increasing selectivity.
330 XPS is one of the crucial surface analytical techniques to provide useful information on the
331 nature of the functional groups and also on the presence of structural defects on the CNT
332 membrane surface. From the XPS results presented Table 4, it appears that in spite of small
333 variations in the relative C/C+O-carbon to carbon with oxygen ratio (change was in the order of
334 ± 0.2), the membranes displayed a good resistance to oxidant chemicals as well as acid and base.
335 For NaOCl treatment, which displayed an only slight change in permeability, only slight
336 decrease on C/C+O ratio was observed in XPS at 2000 mg/L. On the other hand, the NaOH
337 treatment, which resulted in the steadiest increase in the permeability, corresponded to almost no
338 change in C/C+O ratio. The treatment with HCl had mild effect on the permeability and

displayed a slight increase in the C/C+O ratio. These results reflect that in spite of the harsh conditions the membranes displayed a slight surface modification. For hydrochloric acid treatment, a sp^2 hybridized carbon enrichment was reported to take place at the surface, thus forming a protective barrier against chlorine degradation and fouling [37]. Taking into account that whole membranes display some natural irregularities (assays were performed in 44.5 mm coupons, the size of a 50 mL Amicon stirred cells, although multiple replicates were analyzed for each case), it can be concluded that these surface changes are minor. Furthermore, one should consider than in practice membranes will be subjected to considerable milder conditions.

High Resolution-XPS was further performed for evaluating chemical environment of C1s line of the unmodified C80 membranes after exposing membranes to different chemical treatments. Typical deconvolution curves of the HR-XPS C1s lines of the membranes after 24 h exposure to chemicals are shown in Fig. 4 and the different peak attributions are summarized in Table 5. After deconvolution, the C1s line showed a main peak at 284.1 eV (peak#A) that was attributed to the graphitic structure (sp^2 hybridized). The peak at 285.5 eV (peak#B) was either attributed to sp^3- hybridized carbon or defects due to carbon atom that are no longer in the original tubular structure, whereas following peaks 286.7 eV (peak#C), and 288.3 eV (peak#D) are indicative of different oxygen based functionalities at the chemical environment of the carbon atoms. Finally the peak#E (at 290.4 eV) is related to π- $\pi*$ transition loss peak. HR-XPS data are summarized in Table 5 with the different peak attributions and the proportional peak area ratios. After the membrane was exposed to 2N HCl no significant changes could be observed comparing to the reference sample. Similar results were observed for membranes after exposure to NaOCl or NaOH. XPS results and peak attribution are in good agreement [37].

Overall, results of the chemical resistance tests indicate that CNT membranes are very resistant, even to harsh conditions. It should be noted that the fact that the membranes are monolithic, all made of CNTs, presents the advantage of uniform and high overall chemical resistance and electrical conductivity. Although some slight sign of oxidation appear upon prolonged exposure to excessively high chemicals dose, one may expect from these membranes to be very resistant to chemical cleaning and cleaning-in-place treatments that are common in industrial applications. These results further indicate that exposure to harsh chemical conditions did not modify the performance of the membranes, neither in terms of permeability nor in terms of selectivity.

In addition to the chemical stability, the intrinsic antibacterial ability of CNT membranes was estimated in cross-flow filtration under conditions encouraging biofouling with a pure culture of a model bacterium and compared with a commercial Psf UF membrane. HRSEM micrographs after approx. 72 h filtration and corresponding permeability data suggest relatively good antibacterial response (Fig. S5). Indeed, only sporadic attached bacteria with no biofilm layer developed on the CNT surface in contrast to a well-developed biofilm on the Psf surface, in line with previous studies [18, 20]. The effect on membrane permeability during biofouling test, although somewhat less impressive, was still considerable, especially considering the different MWCO of both membranes (65 and 200 kDa for CNT and Psf, respectively). The most marked difference could be seen after the first 24 h, once biofilm developed. Although the intrinsic antibacterial activity of CNTs in a mat or fabric is not yet fully understood, physicochemical interactions between the surface and the microorganism, i.e., electron transfer, may lead to generation of reduced oxygen species placing the cell under oxidative stress. These interactions are thought to be emanated from the graphitic-like structure, i.e., sp^2 carbon atoms lattice, influenced by several factors such as length, residual catalyst, electronic structure, etc. [38].

Nevertheless, active biofouling control through application of low voltage-electrical field taking advantage of the high electrical conductivity of these membranes (≥40,000 S/m) can be successfully manipulated, as we recently reported [3].

4. Conclusions

The filtration capabilities, hydraulic properties and chemical resistance of support-free CNT membranes were characterized. The molecular weight cut-off of the membranes correspond to the selectivity range of tight UF membranes (nominal pore rating about 12-23 nm). The CNT membranes tested displayed outstanding properties comprising very high permeability of 120-400 LMH/bar, one order of magnitude higher for the same separation selectivity of most existing commercial polymeric UF membranes. It appears that this high selectivity regardless of the high permeability may be due to hindered convection of particles, i.e., adsorption and tortuosity, across the whole thickness of the non-woven membranes (by average 25-50 μm). The physical (stretching) and chemical modification (acetone densification) improved intrinsic percolation, selectivity and tortuosity. This is probably due to the increased van der Waals interaction between CNT fibers upon treatment, resulting in a higher rejection thus increasing selectivity. Post-synthesis modification of the laminates, either chemical or physical, can be manipulated to improve permeability and tortuosity, and to certain extent also selectivity. Membranes displayed the added benefit of high chemical resistance to typical chemicals used for membrane cleaning in filtration, including HCl, NaOH and NaClO at long-term exposure and high concentration. This combination of features offers a worthwhile opportunity of application in the UF range, and especially at harsh conditions such as wastewater treatment and purification (effluents filtration, MBR). Moreover, these CNT membranes display intrinsic antibacterial properties and high electrical conductivity that can be applicable for biofouling control. Considering in addition to all

the aforementioned properties, the simplicity of fabrication and easy of post-synthesis modification of the dense-array of tubes, these CNT membranes have the potential to tackle the present and future challenges in water and wastewater treatment and purification.

Acknowledgements

This work was funded by the NOFAR program, Ministry of Commerce, Israel and supported in part at the Technion by a Technion-Guangdong Fellowship. Russell Berrie Nanotechnology Institute (RBNI) at Technion is gratefully acknowledged for their kind support. Authors gratefully acknowledged TorTech Nano Fibers Ltd for kindly synthesizing and providing the CNT laminates. We thank Alina Shayevich for the technical assistance.

References

[1] J.N. Wang, X.G. Luo, T. Wu, Y. Chen, High-strength carbon nanotube fibre-like ribbon with high ductility and high electrical conductivity, Nat. Commun., 5 (2014) 3848-3856.

[2] C. Kingston, R. Zepp, A. Andrady, D. Boverhof, R. Fehir, D. Hawkins, J. Roberts, P. Sayre, B. Shelton, Y. Sultan, V. Vejins, W. Wohlleben, Release characteristics of selected carbon nanotube polymer composites, Carbon, 68 (2014) 33-57.

[3] C. Thamaraiselvan, A. Ronen, S. Lerman, M. Balaish , Y. Ein-Eli, C.G. Dosoretz, Low voltage electric potential as a driving force to hinder biofouling in self-supporting carbon nanotube membranes, Water Res., 129 (2018) 143-153.

[4] S. Kar, R.C. Bindal, P.K. Tewari, Carbon nanotube membranes for desalination and water purification: Challenges and opportunities, Nano Today, 7 (2012) 385-389.

[5] Q. Li, S. Mahendra, D.Y. Lyon, L. Brunet, M.V. Liga, Antimicrobial nanomaterials for water disinfection and microbial control: Potential applications and implications, Water Res., 42 (2008) 4591-4602.

[6] S. Kang, M. Herzberg, D.F. Rodrigues, M. Elimelech, Antibacterial effects of carbon nanotubes: size does matter!, Langmuir, 24 (2008) 6409-6413.

[7] L.M. Pasquini, S.M. Hashmi, T.J. Sommer, M. Elimelech, J.B. Zimmerman, Impact of surface functionalization on bacterial cytotoxicity of single-walled carbon nanotubes, Environ. Sci. Technol. , 46 (2012) 6297-6305.

[8] R. Das, M.E. Ali, S.B.A. Hamid, S. Ramakrishna, Z.Z. Chowdhury, Carbon nanotube membranes for water purification: A bright future in water desalination, Desalination, 336 (2014) 97-109.

[9] C.H. Ahn, Y. Baek, C. Lee, S.O. Kim, S. Kim, S. Lee, S.-H. Kim, S.S. Bae, J. Park, J. Yoon, Carbon nanotube-based membranes: Fabrication and application to desalination, J. Ind. Eng. Chem., 18 (2012) 1551-1559.

[10] S. Wang, S. Liang, P. Liang, X. Zhang, J. Sun, S. Wu, X. Huang, In-situ combined dual-layer CNT/PVDF membrane for electrically-enhanced fouling resistance, J. Memb. Sci., 491 (2015) 37-44.

[11] F.-Y. Zhao, Q.-F. An, Y.-L. Ji, C.-J. Gao, A novel type of polyelectrolyte complex/MWCNT hybrid nanofiltration membranes for water softening, J. Memb. Sci., 492 (2015) 412-421.

[12] Y. Zhao, Z. Zhong, Z.-X. Low, Z. Yao, A multifunctional multi-walled carbon nanotubes/ceramic membrane composite filter for air purification, RSC Adv. , 5 (2015) 91951-91959.

[13] H.J. Kim, M. Lim, K.H. Jung, D. Kim, J. Lee, High-performance reverse osmosis nanocomposite nanotubes and graphene oxides, J. Mater. Chem. A., 3 (2015) 6798-6809.

[14] Ihsanullah, T. Laoui, A.M. Al-Amer, A.B. Khalil, A. Abbas, M. Khraisheh, M.A. Atieh, Novel anti-microbial membrane for desalination pretreatment: A silver nanoparticle-doped carbon nanotube membrane, Desalination, 376 (2015) 82-93.

[15] P. Gunawan, C. Guan, X. Song, Q. Zhang, S. Su, J. Leong, Hollow fiber membrane decorated with Ag/MWNTs: Toward effective water, ACS Nano, 5 (2011) 10033-10040.

[16] J.K. Holt, H.G. Park, Y. Wang, M. Stadermann, A.B. Artyukhin, C.P. Grigoropoulos, A. Noy, O. Bakajin, Fast mass transport through sub-2-nanometer carbon nanotubes, Science, 312 (2006) 1034-1037.

[17] A. Srivastava, O.N. Srivastava, S. Talapatra, R. Vajtai, P.M. Ajayan, Carbon nanotube filters, Nat. Mater., 3 (2004) 610-614.

[18] Y. Baek, C. Kim, D.K. Seo, T. Kim, J.S. Lee, Y.H. Kim, K.H. Ahn, S.S. Bae, S.C. Lee, J. Lim, K. Lee, J. Yoon, High performance and antifouling vertically aligned carbon nanotube membrane for water purification, J. Memb. Sci., 460 (2014) 171-177.

[19] F. Du, L. Qu, Z. Xia, L. Feng, L. Dai, Membrane of vertically aligned superlong carbon nanotubes, Langmuir, 27 (2011) 8437-8443.

[20] B. Lee, Y. Baek, M. Lee, D.H. Jeong, H.H. Lee, J. Yoon, Y.H. Kim, A carbon nanotube wall membrane for water treatment, Nat. Commun., 6 (2015) 7109.

[21] M. Yu, H.H. Funke, J.L. Falconer, R.D. Noble, High density, vertically-aligned carbon nanotube membranes, Nano Lett., 9 (2009) 225-229.

[22] D. Yoon, C. Lee, J. Yun, W. Jeon, B.J. Cha, S. Baik, Enhanced condensation, agglomeration, and rejection of water vapor by superhydrophobic aligned multiwalled carbon nanotube membranes, ACS Nano, 6 (2012) 5980-5987.

[23] G. Wei, S. Chen, X. Fan, X. Quan, H. Yu, Carbon nanotube hollow fiber membranes: High-throughput fabrication, structural control and electrochemically improved selectivity, J. Memb. Sci., 493 (2015) 97-105.

[24] Y.-L. Li, I.A. Kinloch, A.H. Windle, Direct spinning of carbon nanotube fibers from chemical vapor deposition synthesis, Science, 304 (2004) 276-278.

[25] M.F.L. De Volder, S.H. Tawfick, R.H. Baughman, A.J. Hart, Carbon nanotubes: present and future commercial applications, Science, 339 (2013) 535-539.

[26] ASTM E1343-90, Standard test method for molecular weight cutoff evaluation of flat sheet ultrafiltration membranes (Withdrawn 2010), ASTM International, West Conshohocken, PA, (2001) pp: 1-9, doi: 10.1520/e1343-1590r1501.

[27] P. Aimar, M. Meireles, Calibration of ultrafiltration membranes against size exclusion chromatography columns, J. Memb. Sci., 346 (2010) 233-239.

[28] H.P. Erickson, Size and shape of protein molecules at the nanometer level determined by sedimentation, gel filtration, and electron microscopy, Biol. Proced. Online, 11 (2009) 32-51.

[29] G.S. Ajmani, T. Abbott-Chalew, B. Teychene, Y. Wang, J.G. Jacangelo, H. Huang, Effect of hydrodynamic diameter on the sieving of waterborne carbon nanotubes by porous membranes, J. Memb. Sci., 470 (2014) 470-478.

[30] A. Ronen, A. Resnick, S. Lerman, M.S. Eisen, C.G. Dosoretz, Biofouling suppression of modified feed spacers: Localized and long-distance antibacterial activity, Desalination, 393 (2016) 159-165.

[31] W. Zhou, Y. Wu, F. Wei, G. Luo, W. Qian, Elastic deformation of multiwalled carbon nanotubes in electrospun MWCNTs-PEO and MWCNTs-PVA nanofibers, Polymer, 46 (2005) 12689-12695.

[32] Q. Zhang, W. Zhou, W. Qian, R. Xiang, J. Huang, D. Wang, F. Wei, Synchronous growth of vertically aligned carbon nanotubes with pristine stress in the heterogeneous catalysis process, J. Phys. Chem. C., 111 (2007) 14638-14643.

[33] H.J. Butt, B. Cappella, M. Kappl, Force measurements with the atomic force microscope: Technique, interpretation and applications, Surf. Sci. Rep., 59 (2005) 1-152.

[34] Z. Rahimi, L. Zinatizadeh, S. Zinadini, Preparation of high antibiofouling amino functionalized MWCNTs/PES nanocomposite ultrafiltration membrane for application in membrane bioreactor, J. Ind. Eng. Chem., 29 (2015) 1-9.

[35] T.-Y. Liu, Y. Tong, Z.-H. Liu, H.-H. Lin, Y.-K. Lin, B. Van der Bruggen, X.-L. Wang, Extracellular polymeric substances removal of dual-layer (PES/PVDF) hollow fiber UF membrane comprising multi-walled carbon nanotubes for preventing RO biofouling, Sep. Purif. Technol., 148 (2015) 57-67.

[36] X. Yao, J. Li, Z. Wang, L. Kong, Y. Wang, Highly permeable and robust membranes assembled from block-copolymer-functionalized carbon nanotubes, J. Memb. Sci., 493 (2015) 224-231.

[37] S. Inukai, R. Cruz-Silva, J. Ortiz-Medina, A. Morelos-Gomez, K. Takeuchi, T. Hayashi, A. Tanioka, T. Araki, S. Tejima, T. Noguchi, M. Terrones, M. Endo, High-performance multi-functional reverse osmosis membranes obtained by carbon nanotube·polyamide nanocomposite, Sci. Rep., 5:13562 (2015) doi:10.1038/srep13562.

[38] A. Al-Jumaili, S. Alancherry, K. Bazaka, M.V. Jacob, Review on the antimicrobial properties of carbon nanostructures, Materials, 10:1066 (2017) doi:10.3390/ma10091066.

Figure Legends

Figure 1. Normalized permeability at 20℃ of CNT membranes. Left: Unmodified; Middle:Stretched; Right: Acetone densified. Symbols are experimental data and lines represent linear fit. J^{20}: normalized permeate flux at 20℃; ΔP: transmembrane pressure. See Table 1 for linear fit parameters. Data represent average±standard deviation of at least three-six independent experiments.

Figure 2. Semi-logarithmic plot of rejection *vs*. molecular weight for the C-80 unmodified membrane using globular proteins (17-670 kDa), blue dextran (2,000 kDa) and fluorescent beads (40-900 nm) markers. ●: empirical data; —: fit to Ferry-Renkin equation (Eq. 6). Data represent average±standard deviation of at least three replicates.

Figure 3. Relative change in pore rating of C-80 membranes before and after chemical resistance tests. Values represent relative values towards the control (untreated). Pore rating was calculated according to Eqs. 4-6. Pore rating of untreated (control) membranes are given in Table 1.

Figure 4. Typical deconvolution of the XPS C1s lines of the CNT unmodified C-80 membranes after 24 h exposure to chemicals. (a) Control (untreated), (b) 2N HCl, c) 2000 ppm NaOCl, d) 2N NaOH. See Table 5 for details of relative ratio of the peak surface area and transition loss peak π- π* peak.

Table 1. Properties of CNT membranes tested in the research.

Membrane	**Thickness (µm)**	**Average Permeability$^{@20°C}$ (LMH/bar)[a]**	**Nominal pore rating (nm)[b]**
C-171	50	458±77	na
C-171 str	45	379±43	20
C-171 actD	50	281±26	20
C-162 str	50	163±23	23
C-162 actD	65	120±11	14
C-80	60	352±60	23
C-80 str	25	330±41	12
C-80 actD	51	240±7	19

[a]Calculated according to Eq. 1-3 at 20°C. Values represent average±standard deviation of at least 3 replicates.

[b]Calculated according to Eqs. 4-6 for 90% rejection. na: not analyzed.

str: Stretched; actD: Acetone densified.

Table 2. Structural morphology characteristics of C-80 membranes[a].

Membrane	**MWCO (kDa)**	**Tortuosity factor (l_0/le)**	**Average Roughness (nm)**	**Mean square Root roughness (nm)**	**Contact angle (θ)**
Unmodified	65	2.76±1.37	18.7±7.9	24.0±10.2	102.2±6.7
Stretched	18	2.39±1.45	34.2±3.0	43.5±3.5	78.3±7.1
Acetone densified	26	1.75±0.50	22.6±7.9	28.0±9.1	118.1±9.1

[a]Values represent average±standard deviation of at least 3 replicates.

Table 3. Post-treatment permeability of different CNT membranes following chemical resistance tests[a].

Treatment	**NaClO 0.5 g/L**		**NaClO 1 g/L**		**NaClO 2 g/L**		**NaOH 2 N**		**HCl 2 N**	
Time (h)	1	24	1	24	1	24	1	24	1	24
C-171	0.97±0.02	1.04±0	0.88±0.11	1.1±0.02	1.01±0.02	0.99±0.01	1.00±0.02	1.06±0.01	1.03±0.04	1.03±0.02
C-171 s	1.00±0.02	1.05±0.02	0.99±0.09	1.05±0.02	0.97±0.03	0.93±0.03	1.15±0.02	1.16±0.01	0.98±0.03	1.01±0.04
C-171 actD	0.98±0.01	1.01±0.01	0.99±0.01	1.1±0.01	0.95±0.03	0.94±0.02	1.12±0.01	1.11±0.03	1.06±0.02	1.22±0.06
C-162 str	0.98±0.01	1.02±0.02	0.96±0.03	1.05±0.01	1.00±0.01	1.05±0.05	1.13±0.00	1.10±0.02	1.01±0.00	1.01±0.02
C-162 actD	1.04±0.03	1.06±0.01	1.00±0.01	1.03±0.00	1.08±0.02	1.07±0.02	1.14±0.02	1.12±0.01	1.10±0.05	1.09±0.00
C-80	0.96±0.03	1.01±0.02	0.92±0.03	0.98±0.04	1.03±0.02	1.05±0.02	1.17±0.02	1.16±0.01	1.15±0.01	1.11±0.03
C-80 str	0.97±0.03	1.10±0.01	1.00±0.04	1.12±0.02	1.00±0.03	0.94±0.03	1.14±0.01	1.13±0.01	1.06±0.04	1.16±0.02
C-80 actD	0.96±0.01	1.02±0.01	1.04±0.01	1.08±0.02	0.99±0.01	1.05±0.02	0.91±0.02	1.13±0.02	1.01±.02	1.01±0.02

[a]Data represent relative permeability with regards to the initial permeability (t=0) before treatments (controls).

str: Stretched; actD: Acetone densified.

Table 4. Elemental surface composition (in %) based on XPS analysis of unmodified CNT C-80 membranes before (control) and after chemical resistance tests.

Elements	C	O	Fe	Si	Na	Cl	C/C+O
Control	94.46	4.73	0.32	0.49	nd	nd	0.95
2NHCl	95.97	3.73	0.30	nd	nd	nd	0.97
2000 ppm NaOCl	91.68	6.89	0.48	nd	0.71	0.25	0.93
2N NaOH	95.22	4.49	0.29	nd	nd	nd	0.95

nd: not detected.

Table 5. Summarizing data of HR-XPS C1s line of peak location (nm) and relative ratio of peak surface area of unmodified C-80 membranes before (control) and after chemical resistance tests.

Sample	**XPS data**	**Peak#A C- sp2**	**Peak#B C sp3 and defects**	**Peak#C C-O**	**Peak#D Carbonates**	**Peak#E π- π***
Control	Binding Energy (eV)	284.1	285.5	286.7	288.3	290.4
	Peak Area Ratio (%)	73.8	13.5	6.0	2.5	4.2
2N HCl	Binding Energy (eV)	284.0	285.2	286.9	289.7	290.4
	Peak Area Ratio (%)	73.5	13.2	6.4	3.0	3.9
NaOCl	Binding Energy (eV)	284.1	285.2	286.4	288.4	290.2
	Peak Area Ratio (%)	74.1	13.5	5.6	3.4	3.4
NaOH	Binding Energy (eV)	284.1	285.2	286.4	288.7	289.9
	Peak Area Ratio (%)	72.4	12.5	6.2	3.5	5.4

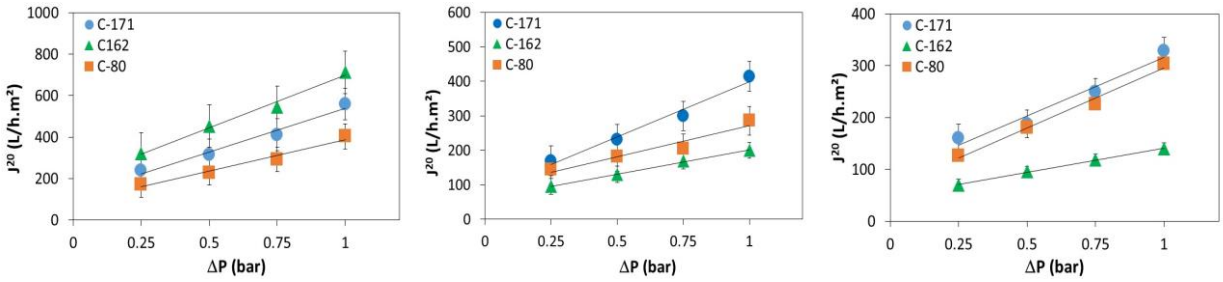

Fig. 1

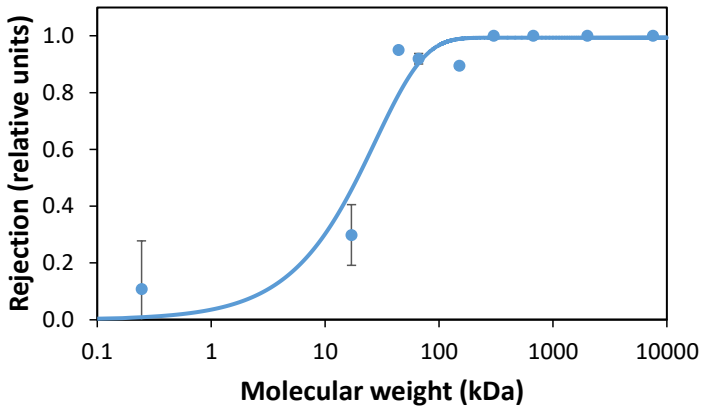

Fig. 2

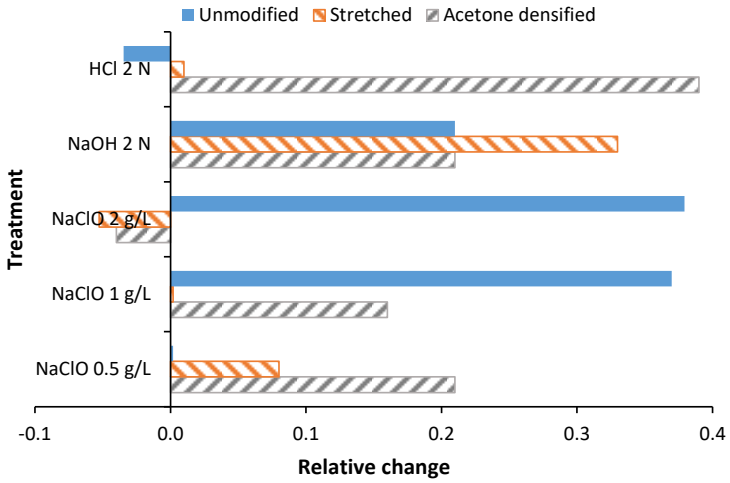

Fig. 3

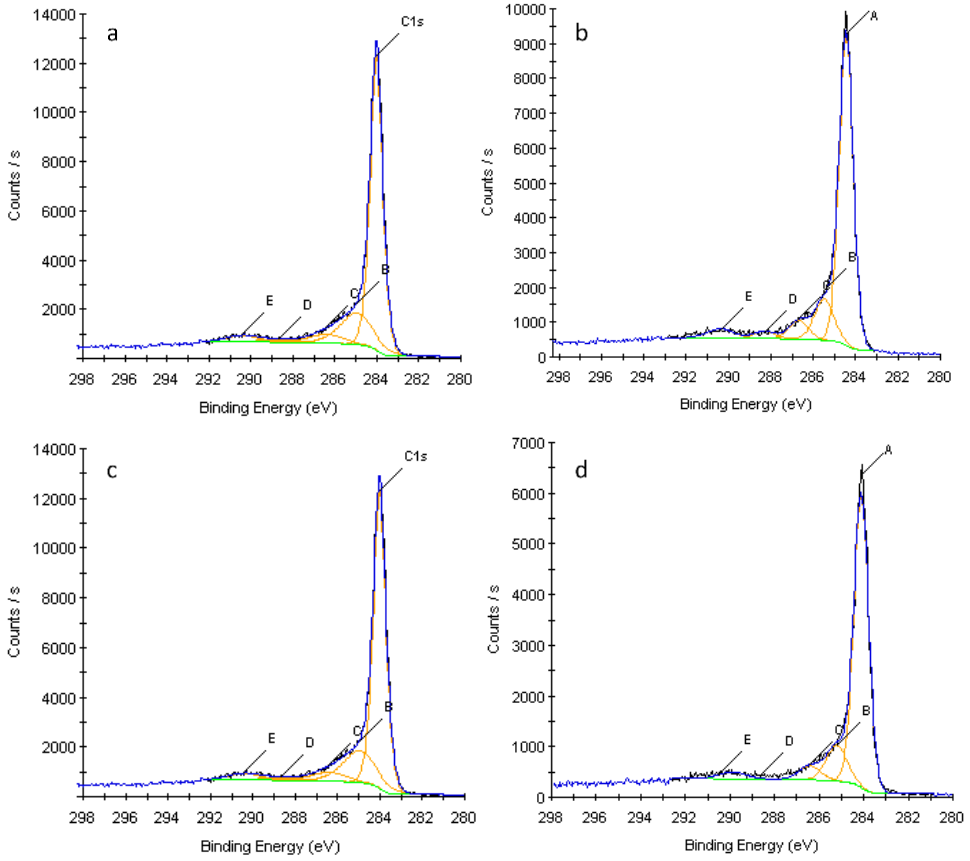
a
C1s
E
D
C
B
Counts / s
Binding Energy (eV)
b
A
E
D
C
B
Counts / s
Binding Energy (eV)
c
C1s
E
D
C
B
Counts / s
Binding Energy (eV)
d
A
E
D
C
B
Counts / s
Binding Energy (eV)

Fig. 4